Observation of Anomalous π Modes in Photonic Floquet Engineering

Qingqing Cheng,[1] Yiming Pan,[2,*] Huaiqiang Wang,[3,†] Chaoshi Zhang,[1] Dong Yu,[1] Avi Gover,[2] Haijun Zhang,[3,4] Tao Li,[3,4] Lei Zhou,[5,4] and Shining Zhu[3,4,‡]

[1]*Shanghai Key Lab of Modern Optical System and Engineering Research Center of Optical Instrument and System (Ministry of Education), University of Shanghai for Science and Technology, Shanghai 200093, China*
[2]*Department of Electrical Engineering Physical Electronics, Tel Aviv University, Ramat Aviv 69978, Israel*
[3]*National Laboratory of Solid State Microstructures, School of Physics, College of Engineering and Applied Sciences, Nanjing University, Nanjing 210093, China*
[4]*Collaborative Innovation Center of Advanced Microstructures, Nanjing 210093, China*
[5]*Department of Physics, Fudan University, Shanghai 200433, China*

(Received 31 August 2018; revised manuscript received 20 February 2019; published 3 May 2019)

Recent progress on Floquet topological phases has shed new light on time-dependant quantum systems, among which one-dimensional (1D) Floquet systems have been under extensive theoretical research. However, an unambiguous experimental observation of these 1D Floquet topological phases is still lacking. Here, by periodically bending an ultrathin metallic array of coupled corrugated waveguides, a photonic Floquet simulator was well designed and successfully fabricated to mimic the periodically driven Su-Schrieffer-Heeger model. Intriguingly, under moderate driven frequencies, we report the first observation of the anomalous Floquet topological π mode, propagating along the array's boundary. The different evolutionary behaviors between static and nonstatic topological end modes have been clearly demonstrated by the microwave near-field experiment. Furthermore, the experiment in the fast-driving regime also reveals the universal high-frequency behavior in driven systems. Our photonic simulator can serve as a versatile testing ground for various phenomena related to time-dependant 1D quantum phases, such as Thouless pumping and dynamical localization.

DOI: 10.1103/PhysRevLett.122.173901

Introduction.—Recently, following the development of topological insulators [1,2], it has been shown that periodic perturbations (or modulations) can be used to realize new engineered topologically nontrivial phases not accessible in static equilibrium systems. This promising area of research, termed as "Floquet engineering" [3–10], has motivated growing interest in periodically driven quantum systems, and has been employed in condensed-matter systems [11–14], ultracold atom optical lattices [15,16], spin systems [4,9], time crystals [17–20], and photonic simulations [21–27]. Intriguingly, recent theoretical studies have demonstrated that the Floquet quasienergy spectra of periodically driven systems exhibit richer topological structures and invariants than their nondriven counterparts [28–44], attaching to the gaps of quasienergy bands, such as Floquet-Majorana end states [45–48], topologically nontrivial zero or π states [33–35], and topological singularities [37]. However, finding materials that hold such Floquet-engineered topological phases remains a serious challenge in condensed-matter physics [3,4,49,50].

Inspired by great successes in discoveries of topological phenomena in artificial quantum systems, such as ultracold atoms and photonic systems [51–54], many researchers have begun to explore experimental possibilities of achieving nonstatic engineered topological states in these systems with high structural flexibility and tunability. For example, two-dimensional (2D) photonic and phononic Floquet topological phases (FTPs) have already been realized [55–57], with clear observations of Floquet topological edge states. However, experimental realizations of the seemingly simpler one-dimensional (1D) FTP are still rare, not to mention an unambiguous demonstration of corresponding 1D anomalous Floquet end modes (FEMs). Moreover, the realistic dynamic evolution of the FEMs has remained unclear so far, though it is assumed to be different from its static counterpart.

To address these problems, in this Letter, we designed and fabricated a photonic Floquet simulator (PFS) to mimic a typical 1D Floquet system, namely, the periodically driven Su-Schrieffer-Heeger (SSH) model [33–35], through periodically bending ultrathin metallic arrays of coupled corrugated waveguides, which support spoof surface plasmon polaritons at microwave to infrared wavelength. By adjusting the bending profiles of the waveguide array and the initial field inputs, the Floquet topological π mode was experimentally observed and theoretically verified, which propagates along the array's boundary. We also give a clear demonstration of the different evolutionary behaviors between the anomalous π mode and its static counterpart end mode (i.e., zero mode). In addition, in the fast-driving

regime, our simulator reveals the universal high-frequency behavior prevailing in Floquet engineering [3]. Our PFS provides a versatile platform for investigating various phenomena related to time-dependant 1D quantum systems, such as Thouless pumping of light [58], and dynamical localization [16].

Periodically driven SSH model.—The original SSH model [59] is a well-known 1D topological structure with two degenerate ground states differing by the relative strength between intracell and intercell hoppings. To study the periodically driven SSH model, we bend the waveguides periodically along their propagating direction z which now acts as the synthetic time dimension [55]. As illustrated in Fig. 1(a), two neighboring waveguides are coupled with opposite axis offsets, $x_0(z) = \pm A_0 \cos[(2\pi z/\Lambda) + \theta_0]$, where A_0 ($= 0.8$ mm) and Λ denote the amplitude and period of the sinusoidal bending, respectively, and θ_0 is the initial phase determined by the starting "time" z_0. Through the coupled-mode theory [21,25,60–62], the waveguide array can be mapped into an effective 1D time-periodic tight-binding-approximated Hamiltonian as

$$H(z) = \sum_{i=1}^{N} \beta_i(z) c_i^\dagger c_i + \sum_{i=1}^{N-1} (\kappa_0 + (-1)^i \Delta\kappa(z)) c_i^\dagger c_{i+1} + \text{H.c.} \tag{1}$$

Here, N is the number of waveguides, $\beta_i(z)$ is the effective propagation constant which can be reasonably treated as a constant in the weak-guidance approximation (WGA) [21,25,62]. For simplicity, this constant shift term will be safely neglected in the theoretical analysis. The second term in Eq. (1) represents couplings between nearest-neighbor (NN) waveguides with a constant (staggered) coupling strength κ_0 ($\Delta\kappa(z)$). According to the WGA, the NN coupling strength κ mainly depends on their distance $G(z)$, with the relation shown in Fig. 1(b). In our configuration, the NN spacing $G(z) = g_0 \pm 2A_0 \cos[(2\pi z/\Lambda) + \theta_0]$, where g_0 (≈ 2.6 mm) is the initial spacing without bending.

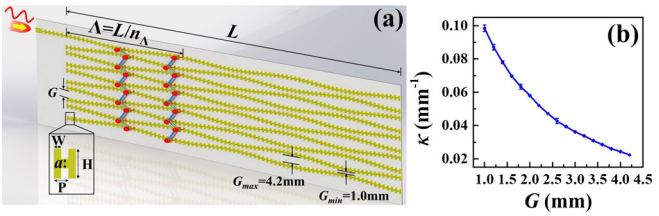

FIG. 1. (a) Schematic illustration of periodically bent ultrathin metallic waveguides, with a cosine modulation of the spacing G between two adjacent waveguides in the propagation direction z. Inset: Illustration of the "H"-shape structure, with the parameters given by $P = 2$ mm, $H = 4$ mm, $a = 0.8$ mm, and $W = 1$ mm. (b) The effective coupling constant κ as a function of G for the input microwave field with frequency 17 GHz.

Consequently, κ can be approximated as $\kappa_0 \pm \delta\kappa \cos[(2\pi z/\Lambda) + \theta_0]$, with the optimal parameters given by $\kappa_0 \approx 0.042$ mm^{-1} and $\delta\kappa \approx 0.02$ mm^{-1}. Note that the staggered term $\Delta\kappa(z)$ is periodically modulated, and the Hamiltonian $H(z)$ in Eq. (1) thus exactly mimics the periodically driven SSH model with tunable time-periodic NN couplings.

Experimental results.—In our experiments, ten waveguides were coupled into an array with propagation distance $L = 400$ mm (numerical simulations of the $L = 800$ mm waveguides are provided in the supplemental materials [62]). The driven frequency is given by $\omega \equiv 2\pi/\Lambda = n_\Lambda \omega_L$, where Λ corresponds to the bending period, n_Λ is the total number of periods within L, and the characteristic frequency is defined as $\omega_L \equiv (2\pi/L)$. For fixed L, n_Λ was adjusted to investigate various frequency-dependent nonstatic phenomena related to the driven SSH model [33–35]. Additionally, unless otherwise specified, we set $\theta_0 = 0$.

We start from the high frequency limit where the bending period Λ is much smaller than the effective coupling length. In this case, the time-periodic staggered NN coupling is smeared out due to its fast oscillating behavior, thus rendering the system similar to that composed of straight waveguides with identical NN couplings, which obviously belongs to the trivial phase [62]. A waveguide array with a representative $\omega = 20\omega_L$ (≈ 0.314 mm^{-1}) in this high-frequency range was fabricated, as illustrated in Fig. 2(a), to carry out the near-field measurement of the amplitude profile after injecting a microwave of 17 GHz from the upmost boundary waveguide. As expected, this field evolution pattern resembles that of straight coupled waveguides with identical NN couplings, as presented in Fig. 2(b) for comparison. The minor differences between local details of propagation patterns for the two cases may stem from imperfect "H"-shape structures in the fast-varying bending profile (see Fig. S8 [62]). Note that the high-frequency driving is a "do-nothing" effect here, in contrast to the case of dynamic localization obtained in high-frequency driven quantum-mechanical lattice models with electromagnetic fields [16].

Intriguingly, as we gradually decrease the driven frequency to the range $\omega = 2 \sim 5\omega_L$ (i.e., 0.0314–0.0785 mm^{-1}), a quite distinct propagation field pattern arises along the array's boundary, as exemplified by the $\omega = 3\omega_L$ (0.0471 mm^{-1}) structure with corresponding experimental results in Fig. 2(c). The injected microwave no longer spreads into the bulk array, but instead is mainly localized within the two waveguides at the upper boundary. The localized field profile exhibits a periodic oscillation pattern in its distribution between the two boundary waveguides. This anomalous edge mode is the central achievement of our work, which will be theoretically proved as the long pursued Floquet π mode predicted in the Floquet SSH model [33–35]. To further reveal its difference from the well-known zero-mode edge state of the static SSH model, we fabricated an array of dimerized straight waveguides

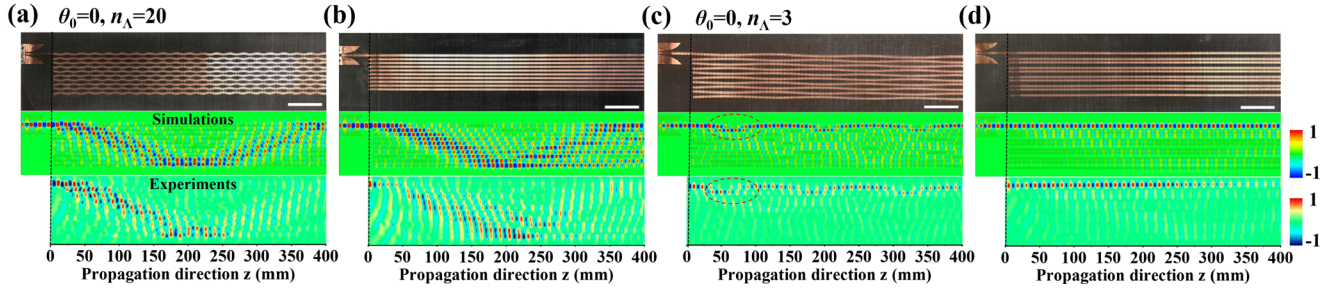

FIG. 2. (From up to down in each figure) Snapshots of the fabricated samples, simulations by the CST microwave studio simulation software, and near-field measurement of the field profile after injecting the microwave from the upmost boundary waveguide, under different driving conditions with the same length $L = 400$ mm, waveguide number $N = 10$, and initial phase $\theta_0 = 0$. Results for curved waveguides with (a) $n_\Lambda = 20$ and (c) $n_\Lambda = 3$, and for straight waveguides ($n_\Lambda = 0$) with (b) identical spacings $G = 2.5$ mm and (d) dimerized spacings between NN waveguides.

with time-independent staggered NN couplings [see Fig. 2(d)], which lies in the topologically nontrivial phase [25,59]. The experimental measurement in Fig. 2(d) shows that the injected microwave always propagates along the boundary waveguide without scattering into the bulk or displaying any oscillation in its amplitude distribution, in striking contrast to the nonstatic edge mode.

Theoretical analysis.—To verify the existence of the anomalous edge mode, we explicitly calculate the topological invariant of the quasienergy spectrum of our system to determine its phase diagram by using Floquet theory. The time evolution operator of the system is given as $U(z, z_0) = \hat{T} e^{-i\int_{z_0}^{z} H(z')dz'}$, where $\hat{T}$ denotes the time-ordering operator, and z_0 is the initial time. Without loss of generality, we set $z_0 = 0$ and $U(z, z_0) = U(z)$ to simplify notations. The Floquet operator is defined as the time evolution operator for one full period, given by $U(\Lambda)$ [50], from which a time-averaged effective Hamiltonian can be defined as $H_F = (i/\Lambda)\ln U(\Lambda)$ [50]. The eigenvalues of H_{eff} correspond to the quasienergy spectrum of the system. Because of the translation symmetry, both $U(z)$ and H_F can be Bloch decomposed as $U_z = \prod U(z, k)$ and $H_F = \sum_k H_F(k)$, respectively. According to Ref. [35], a $\mathbb{Z}$-valued invariant can be defined for the quasienergy gap at zero or π for a 1D periodically driven system with chiral symmetry, as also satisfied for our model. To calculate this invariant, we resort to the periodized evolution operator, given by $V(z, k) \equiv U(z, k)e^{iH_F(k)z}$. It is found that regardless of the value of ω, no gap appears around quasienergy zero in our model, so we only need to calculate the π gap invariant G_π through [35]

$$G_\pi = \frac{i}{2\pi}\int_{-\pi}^{\pi} \text{tr}((V_\pi^+)^{-1}\partial_k V_\pi^+)dk, \tag{2}$$

where V_π^+ is obtained from $V(z, k)$ at half period:

$$V(\Lambda/2, k) = \begin{pmatrix} V_\pi^+ & 0 \\ 0 & V_\pi^- \end{pmatrix}. \tag{3}$$

The numerical result of G_π as a function of ω is presented in Fig. 3(b), where the bandwidth of the undriven system $\Delta = 4\kappa_0$ is taken as the energy scale. When $\omega/\Delta > 1$, $G_\pi = 0$, but when $1/3 < \omega/\Delta < 1$, $G_\pi = 1$ (G_π at $\omega/\Delta < 1/3$ is not presented here, since the complex low-frequency behavior may result in unpleasant noninteger values of the topological invariant [10]). A nonzero G_π indicates a topologically nontrivial phase and through bulk-edge correspondence, it corresponds to the number of edge π modes within the π gap [35], as confirmed by the open-boundary quasienergy spectrum in Fig. 3(a), where the waveguide number is $N = 80$, and π modes appear within the range $1/3 < \omega/\Delta < 1$. It should be emphasized that the experimental range of $\omega = 0.0314$–0.0785 mm^{-1}, where anomalous edge modes are observed, approximately falls into this topologically nontrivial region of $\Delta/3 \sim \Delta$ (0.056–0.168 mm^{-1}), thus permitting us to reasonably identify them as the π modes predicted in the periodically driven SSH model.

In fact, the underlying physics becomes much clearer in the direct-product Floquet space: $\mathcal{H} \otimes \mathcal{T}$ [34,36], where $\mathcal{H}$ is the usual Hilbert space and $\mathcal{T}$ denotes the space of time-periodic functions spanned by $e^{in\omega t}$, with the integer index n representing the nth Floquet replica [34]. Considering the periodic nature of the energy, we only need to focus on the energy range $(-\pi, \pi]$ (or $(-(\omega/2), (\omega/2)]$) of the $n = 0$ replica. When $\omega > \Delta$, the $n = 0$ replica is decoupled from other replicas with a gap between the $n = 1$ replica at $\epsilon = \pi$ ($-\pi$ is equivalent to π), which should be topologically trivial since this gap persists when ω approaches the trivial high-frequency limit. At $\omega = \Delta$, as shown in Fig. 3(d) (first column), this gap is closed due to the band touching of the $n = 0$ and 1 replicas at $\epsilon = \pi$. With further decreasing ω, the coupling between $n = 1$ and 0 replicas opens this gap again, as shown in Fig. 3(d) (middle column) with $\omega = \Delta/2$. This gap will close again at $\omega = \Delta/3$, where the $n = 2$ and -1 replicas touch at $\epsilon = \pi$ [last column in Fig. 3(d)]. It has been shown in Ref. [34] that this gap closing-reopening process switches the π gap from trivial to nontrivial through the calculation of the Zak phase [34].

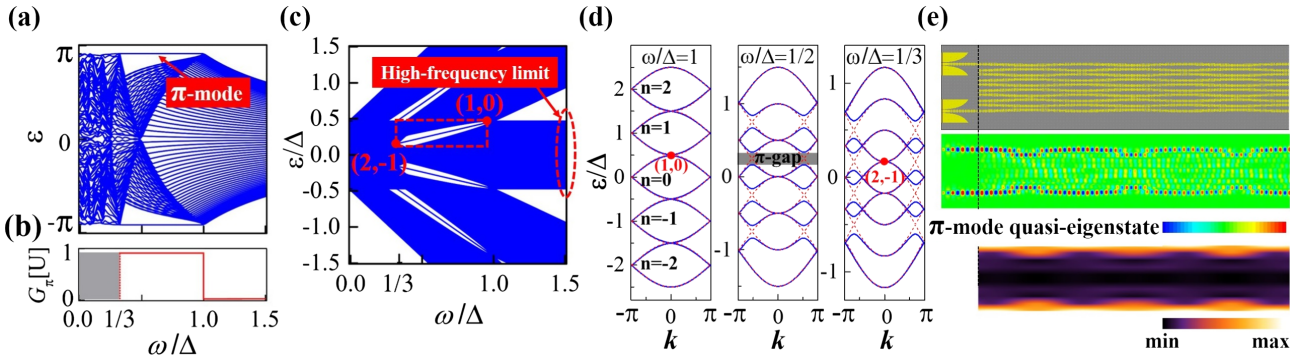

FIG. 3. (a) Quasienergies under open-boundary conditions (OBCs) with 80 waveguides and (b) G_π as a function of the driving frequency ω, where the bandwidth Δ is taken as the energy unit. Floquet π modes can be found in the quasienergy spectrum when $1/3 < \omega/\Delta < 1$ with $G_\pi = 1$. When choosing five frequency replicas $n = 0, \pm 1, \pm 2$. (d) The momentum space quasienergy band structures (blue solid lines) of the five chosen frequency replicas with $\omega/\Delta = 1$ (first column), $\omega/\Delta = 1/2$ (middle column), and $\omega/\Delta = 1/3$ (last column). Red dashed lines correspond to the case with no dimerization ($\delta\kappa = 0$) and uncoupled Floquet replicas, which are used to guide the eye for each Floquet replica. (c) Quasienergies under OBCs with 40 waveguides as a function of ω/Δ. (e) (Bottom row) The dynamic evolution of the π-mode end states for 40 waveguides and $\omega = 3\omega_L$ ($n_\Lambda = 3$), where a ten-waveguide configuration and corresponding CST simulation results are presented in the upper row for reference.

Consequently, the same nontrivial region of $\Delta/3 < \omega < \Delta$ is obtained as above from G_π. When ω is smaller than $\Delta/3$, many more Floquet replicas are involved [34], which is beyond the scope of this Letter. Note that the zero quasienergy gap is always closed regardless of ω, thus eliminating the possibility of the emergence of in-gap zero quasienergy modes. To further support the above argument, we choose $N = 40$ waveguides and $n = 0, \pm 1, \pm 2$ replicas to numerically plot the open-boundary spectrum as a function of ω/Δ in Fig. 3(c) and the time-dependant evolution of the π edge modes with $\omega = 3\omega_L$ in Fig. 3(e) (bottom row). It is obvious that these modes propagate along the array's boundaries and exhibit periodic oscillation in the intensity distribution, which matches well with the CST simulation results presented in Fig. 3(e).

Discussion.—We first discuss the gauge dependence of the initial phase $\theta_0(z_0)$ (i.e., Floquet gauge). The Floquet gauge can be tuned by simply adjusting the initial input position in our structural design. Although the quasienergy and the π mode are theoretically gauge independent, to excite and observe the dynamical π mode, it is found experimentally that θ_0 must be tuned to the region $(-\pi/2, \pi/2)$; i.e., the instantaneous Hamiltonian at the initial time z_0 must lie in the topological nontrivial phase. This is illustrated by our experimental measurements in Figs. 2(c) and 4(a) for $\theta_0 = 0$ and π, respectively, under the same driving frequency $\omega = 3\omega_L$ (results for other θ_0 values are presented in Fig. S4 [62]). In contrast to Fig. 2(c), the injected microwave in Fig. 4(a) no longer propagates along the boundary, but gradually spreads into the bulk array, thus indicating no excitation of the π-mode state. In addition, for the high-frequency case in the topologically trivial phase, the propagating pattern shows no dependence of θ_0, as can be seen by comparing Fig. 2(a) ($\theta_0 = 0$) and Fig. 4(b) ($\theta_0 = \pi$), with the same $\omega = 20\omega_L$. This is related to the universal high-frequency behavior of a periodically driven system [3].

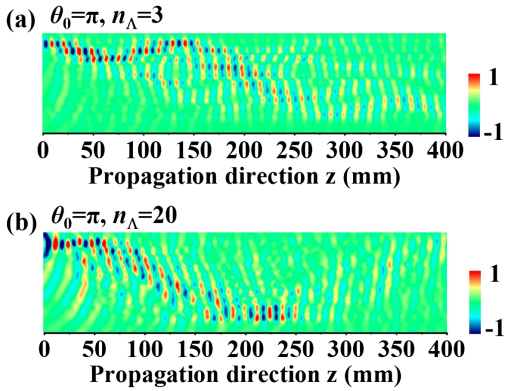

FIG. 4. Near-field measurements of amplitude profiles for 10 waveguides of length $L = 400$ mm, initial phase $\theta_0 = \pi$, and (a) $n_\Lambda = 3$ and (b) $n_\Lambda = 20$.

Next, we examine the topological robustness of the π mode in the presence of weak disorder by introducing weak random coupling coefficients between neighboring waveguides. Through the CST simulation, we present the microwave propagation patterns for $\omega = 3\omega_L$ and $4\omega_L$, respectively, in Figs. S6(a) and S6(b) [62]. It is obvious that the π mode still propagates along the boundary with periodic-driven oscillation and a negligible amount of dissipation into the bulk, which indeed suggests its robustness to weak disorder.

Conclusion.—In summary, by periodically bending ultrathin metallic arrays of coupled corrugated waveguides, we have successfully realized a photonic simulation of the 1D periodically SSH model. Under certain driving protocols and initial input positions, we experimentally observed and theoretically verified the Floquet π mode in 1D periodically driven systems. Because of the extremely high

flexibility and tunability, our Floquet simulator can be widely applied to investigate various driven phenomena in time-dependent quantum systems, including the Thouless pumping [58,63–66] and the possible nonadiabatic Floquet pumping [67].

The authors thank Che-Ting Chan, Ady Arie, Jiangbin Gong, and Koby Scheuer for their helpful discussions and comments. In particular, we thank Xiaopeng Shen for helping us measure the intensity distributions and discuss experiments. This work was supported by the National Natural Science Foundation of China (Grants No. 11604208, No. 11674167, No. 11621091, No. 11322439, No. 11734007, No. 11474057, No. 11674165, No. 11874266, and No. 11674068), Shanghai Science and Technology Committee (Grants No. 16ZR1445600 and No. 16JC1403100), National Key Research and Development Program of China (Grants No. 2017YFA0303701 and No. 2017YFA0303504), the Fok Ying-Tong Education Foundation of China (Grant No. 161006), the Fundamental Research Funds for the Central Universities (No. 020414380038), National Program on Key Basic Research Project (973 Program No. 2015CB352001), and in part by DIP (No. 04340302000) and the US-Israel Binational Science Foundation (No. 00010001000) and the PBC programme of the Israel Council of Higher Education.

Q. C., Y. P., and H. W. contributed equally to this work.

*yimingpan@mail.tau.ac.il
†hqwang@nju.edu.cn
‡zhusn@nju.edu.cn

[1] M. Z. Hasan and C. L. Kane, Rev. Mod. Phys. **82**, 3045 (2010).
[2] X.-L. Qi and S.-C. Zhang, Rev. Mod. Phys. **83**, 1057 (2011).
[3] A. Eckardt and E. Anisimovas, New J. Phys. **17**, 093039 (2015).
[4] M. Bukov, L. D'Alessio, and A. Polkovnikov, Adv. Phys. **64**, 139 (2015).
[5] V. Novičenko, E. Anisimovas, and G. Juzeliūnas, Phys. Rev. A **95**, 023615 (2017).
[6] P. Weinberg, M. Bukov, L. DAlessio, A. Polkovnikov, S. Vajna, and M. Kolodrubetz, Phys. Rep. **688**, 1 (2017).
[7] N. Goldman and J. Dalibard, Phys. Rev. X **4**, 031027 (2014).
[8] V. Khemani, A. Lazarides, R. Moessner, and S. L. Sondhi, Phys. Rev. Lett. **116**, 250401 (2016).
[9] T. Oka and S. Kitamura, Annu. Rev. Condens. Matter Phys. **10**, 387 (2019).
[10] M. Rodriguez-Vega and B. Seradjeh, Phys. Rev. Lett. **121**, 036402 (2018).
[11] T. Oka and H. Aoki, Phys. Rev. B **79**, 081406(R) (2009).
[12] H. Hübener, M. A. Sentef, U. De Giovannini, A. F. Kemper, and A. Rubio, Nat. Commun. **8**, 13940 (2017).
[13] G. E. Topp, N. Tancogne-Dejean, A. F. Kemper, A. Rubio, and M. A. Sentef, Nat. Commun. **9**, 4452 (2018).
[14] J. McIver, B. Schulte, F.-U. Stein, T. Matsuyama, G. Jotzu, G. Meier, and A. Cavalleri, arXiv:1811.03522.
[15] G. Jotzu, M. Messer, R. Desbuquois, M. Lebrat, T. Uehlinger, D. Greif, and T. Esslinger, Nature (London) **515**, 237 (2014).
[16] A. Eckardt, Rev. Mod. Phys. **89**, 011004 (2017).
[17] A. Shapere and F. Wilczek, Phys. Rev. Lett. **109**, 160402 (2012).
[18] F. Wilczek, Phys. Rev. Lett. **109**, 160401 (2012).
[19] D. V. Else, B. Bauer, and C. Nayak, Phys. Rev. Lett. **117**, 090402 (2016).
[20] R. W. Bomantara and J. Gong, Phys. Rev. Lett. **120**, 230405 (2018).
[21] I. L. Garanovich, S. Longhi, A. A. Sukhorukov, and Y. S. Kivshar, Phys. Rep. **518**, 1 (2012).
[22] S. Longhi and K. Staliunas, Opt. Commun. **281**, 4343 (2008).
[23] S. Longhi, Opt. Lett. **30**, 2137 (2005).
[24] S. Longhi, D. Janner, M. Marano, and P. Laporta, Phys. Rev. E **67**, 036601 (2003).
[25] Q. Cheng, Y. Pan, Q. Wang, T. Li, and S. Zhu, Laser Photonics Rev. **9**, 392 (2015).
[26] M. Holthaus, J. Phys. B **49**, 013001 (2016).
[27] B. Zhu, H. Zhong, Y. Ke, X. Qin, A. A. Sukhorukov, Y. S. Kivshar, and C. Lee, Phys. Rev. A **98**, 013855 (2018).
[28] T. Kitagawa, E. Berg, M. Rudner, and E. Demler, Phys. Rev. B **82**, 235114 (2010).
[29] R. Roy and F. Harper, Phys. Rev. B **94**, 125105 (2016).
[30] M. S. Rudner, N. H. Lindner, E. Berg, and M. Levin, Phys. Rev. X **3**, 031005 (2013).
[31] A. C. Potter, T. Morimoto, and A. Vishwanath, Phys. Rev. X **6**, 041001 (2016).
[32] D. V. Else and C. Nayak, Phys. Rev. B **93**, 201103(R) (2016).
[33] J. K. Asbóth, B. Tarasinski, and P. Delplace, Phys. Rev. B **90**, 125143 (2014).
[34] V. Dal Lago, M. Atala, and L. E. F. Foa Torres, Phys. Rev. A **92**, 023624 (2015).
[35] M. Fruchart, Phys. Rev. B **93**, 115429 (2016).
[36] A. Gómez-León and G. Platero, Phys. Rev. Lett. **110**, 200403 (2013).
[37] F. Nathan and M. S. Rudner, New J. Phys. **17**, 125014 (2015).
[38] R. Roy and F. Harper, Phys. Rev. B **96**, 155118 (2017).
[39] T. Iadecola, L. H. Santos, and C. Chamon, Phys. Rev. B **92**, 125107 (2015).
[40] D. Carpentier, P. Delplace, M. Fruchart, and K. Gawedzki, Phys. Rev. Lett. **114**, 106806 (2015).
[41] D. Y. H. Ho and J. Gong, Phys. Rev. B **90**, 195419 (2014).
[42] R. W. Bomantara, G. N. Raghava, L. Zhou, and J. Gong, Phys. Rev. E **93**, 022209 (2016).
[43] S. Yao, Z. Yan, and Z. Wang, Phys. Rev. B **96**, 195303 (2017).
[44] Z. Yan and Z. Wang, Phys. Rev. Lett. **117**, 087402 (2016).
[45] L. Jiang, T. Kitagawa, J. Alicea, A. R. Akhmerov, D. Pekker, G. Refael, J. I. Cirac, E. Demler, M. D. Lukin, and P. Zoller, Phys. Rev. Lett. **106**, 220402 (2011).
[46] M. Thakurathi, A. A. Patel, D. Sen, and A. Dutta, Phys. Rev. B **88**, 155133 (2013).
[47] A. Kundu and B. Seradjeh, Phys. Rev. Lett. **111**, 136402 (2013).

[48] H.-Q. Wang, M. N. Chen, R. W. Bomantara, J. Gong, and D. Y. Xing, Phys. Rev. B **95**, 075136 (2017).
[49] Y. H. Wang, H. Steinberg, P. Jarillo-Herrero, and N. Gedik, Science **342**, 453 (2013).
[50] N. Lindner, G. Refael, and V. Galitski, Nat. Phys. **7**, 490 (2011).
[51] Y. E. Kraus, Y. Lahini, Z. Ringel, M. Verbin, and O. Zilberberg, Phys. Rev. Lett. **109**, 106402 (2012).
[52] A. B. Khanikaev, S. H. Mousavi, W. K. Tse, M. Kargarian, A. H. Macdonald, and G. Shvets, Nat. Mater. **12**, 233 (2013).
[53] A. B. Khanikaev and G. Shvets, Nat. Photonics **11**, 763 (2017).
[54] L. Lu, J. D. Joannopoulos, and M. Soljačić, Nat. Photonics **8**, 821 (2014).
[55] M. C. Rechtsman, J. M. Zeuner, Y. Plotnik, Y. Lumer, D. Podolsky, F. Dreisow, S. Nolte, M. Segev, and A. Szameit, Nature (London) **496**, 196 (2013).
[56] L. J. Maczewsky, J. M. Zeuner, S. Nolte, and A. Szameit, Nat. Commun. **8**, 13756 (2017).
[57] S. Mukherjee, A. Spracklen, M. Valiente, E. Andersson, P. Öhberg, N. Goldman, and R. R. Thomson, Nat. Commun. **8**, 13918 (2017).
[58] Y. Ke, X. Qin, F. Mei, H. Zhong, Y. S. Kivshar, and C. Lee, Laser Photonics Rev. **10**, 995 (2016).
[59] W. P. Su, J. R. Schrieffer, and A. J. Heeger, Phys. Rev. Lett. **42**, 1698 (1979).
[60] W. Huang and H. A. Haus, J. Lightwave Technol. **8**, 922 (1990).
[61] S. Longhi, D. Janner, M. Marano, and P. Laporta, Phys. Rev. E **67**, 036601 (2003).
[62] See Supplemental Material at http://link.aps.org/supplemental/10.1103/PhysRevLett.122.173901 for a detailed description of the coupled-mode theory, high-frequency expansion, finite-size effect and Supplemental Figures.
[63] M. J. Rice and E. J. Mele, Phys. Rev. Lett. **49**, 1455 (1982).
[64] S. Q. Shen, *Topological Insulators: Dirac Equation in Condensed Matters* (Springer Science & Business Media, New York, 2017).
[65] L. Zhou, D. Y. Tan, and J. Gong, Phys. Rev. B **92**, 245409 (2015).
[66] H. Wang, L. Zhou, and J. Gong, Phys. Rev. B **91**, 085420 (2015).
[67] D. Y. H. Ho and J. Gong, Phys. Rev. Lett. **109**, 010601 (2012).